Spin-Crossover in Supramolecular Iron(II)-2,6-bis(1 H-Pyrazol-1-yl)pyridine Complexes Toward Spin-State Switchable Single-Molecule Junctions

Kuppusamy, Senthil Kumar; Mizuno, Asato; García-Fuente, Amador; Van Der Poel, Sebastiaan; Heinrich, Benoît; Ferrer, Jaime; Van Der Zant, Herre S.J.; Ruben, Mario

Important note
To cite this publication, please use the final published version (if applicable).
Please check the document version above.

Spin-Crossover in Supramolecular Iron(II)−2,6-bis(1H-Pyrazol-1-yl)pyridine Complexes: Toward Spin-State Switchable Single-Molecule Junctions

Senthil Kumar Kuppusamy,* Asato Mizuno, Amador García-Fuente, Sebastiaan van der Poel, Benoît Heinrich, Jaime Ferrer,* Herre S. J. van der Zant,* and Mario Ruben*

ACCESS | Metrics & More | Article Recommendations | Supporting Information

ABSTRACT: Spin-crossover (SCO) active iron(II) complexes are an integral class of switchable and bistable molecular materials. Spin-state switching properties of the SCO complexes have been studied in the bulk and single-molecule levels to progress toward fabricating molecule-based switching and memory elements. Supramolecular SCO complexes featuring anchoring groups for metallic electrodes, for example, gold (Au), are ideal candidates to study spin-state switching at the single-molecule level. In this study, we report on the spin-state switching characteristics of supramolecular iron(II) complexes **1** and **2** composed of functional 4-([2,2′-bithiophen]-5-ylethynyl)-2,6-di(1H-pyrazol-1-yl)pyridine (**L1**) and 4-(2-(5-(5-hexylthiophen-2-yl)thiophen-2-yl)ethynyl)-2,6-di(1H-pyrazol-1-yl)pyridine (**L2**) ligands, respectively. Density functional theory (DFT) studies revealed stretching-induced spin-state switching in a molecular junction composed of complex **1**, taken as a representative example, and gold electrodes. Single-molecule conductance traces revealed the unfavorable orientation of the complexes in the junctions to demonstrate the spin-state dependence of the conductance.
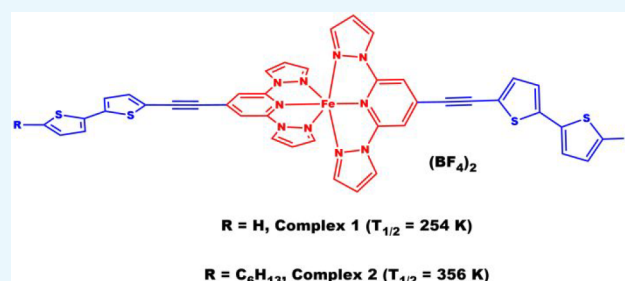
R = H, Complex 1 ($T_{1/2}$ = 254 K)

R = C_6H_{13}, Complex 2 ($T_{1/2}$ = 356 K)

INTRODUCTION

Ever since its genesis dating back to the 1930s,[1] the spin-crossover (SCO) phenomenon[2−7] continually attracted the interest of chemists and physicists alike, and the device suitable characteristics of the SCO systems have been elucidated.[8−11] First-row transition metal complexes featuring a $d^4−d^7$ electronic configuration undergo SCO[12−19] upon application of an external stimulus, for example, temperature, light, or electrical field.[20] While bistable SCO systems showing a thermal hysteresis loop (ΔT) are suitable for fabricating molecule-based switching and memory elements,[21] single-molecule junctions composed of spin-state switchable molecules are useful for developing molecular spintronics elements.[22−30]

Studies on spin-state switching at the bulk and single-molecule levels represent two different paradigms. In the bulk state, intermolecular interactions play a significant role in the spin-state switching process,[31−36] and the switching is often induced by applying temperature as an external stimulus.[3] At the single-molecule level, intermolecular interactions cease to exist, and spin-state switching is achieved by applying a stimulus under isothermal conditions.[37−39] Charging of ligands,[37] electric field-induced distortion of a molecule featuring a large dipole moment,[38] and stretching a molecule in a single-molecule junction[39] are some methods used to induce SCO at the single-molecule level. Electron-induced

spin-state switching at the single-molecule level in surface-bound thin films of SCO active molecules has also been demonstrated in scanning tunneling microscope (STM) junctions at 2 K.[40−44] The spin-state switching at the single-molecule level is accompanied by conductance switching, and high-spin (HS) junctions show a spin-filtering effect,[45,46] elucidating the utility of spin-switchable molecular junctions as molecular spintronics elements.

Supramolecular-SCO systems featuring anchoring groups for electrodes, for example, gold (Au) and single-layer graphene (SLG), are ideal systems to study spin-state switching at the single-molecule level.[24,47] Iron(II) complexes based on 2,6-bis(1H-pyrazol-1-yl)pyridine (BPP) ligand systems[48−50] are suitable systems to study the spin-state dependence of conductance switching at the single-molecule level. Such complexes are remarkable, because BPP ligands feature moderate ligand field strength for iron(II); therefore, SCO is facilitated.[48] Moreover, the pyridine and pyrazole rings of the
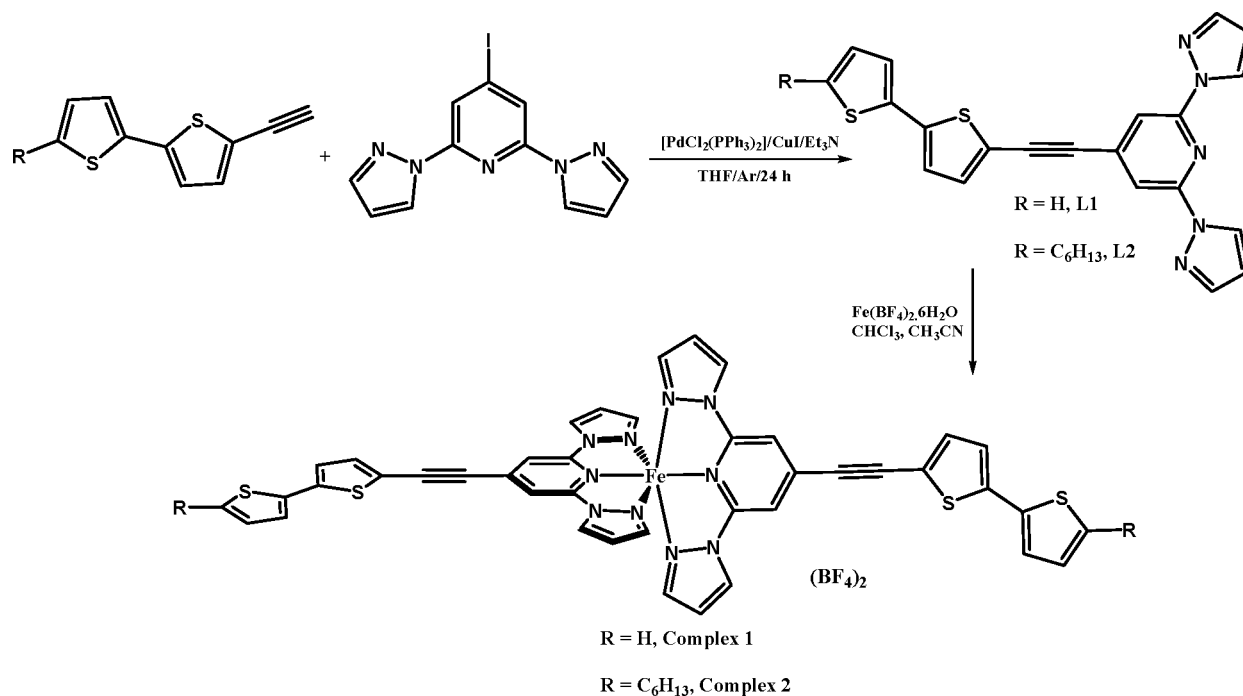
Scheme 1. Syntheses of Ligands L1 and L2 and Complexes 1 and 2 Discussed in This Study

BPP skeleton are amenable to functionalization, enabling the synthesis of functional SCO systems.[51] Consequently, a family of supramolecular BPP ligands featuring thioacetate (SAc), pyrene,[52−54] and fullerene (C60)[53,55,56] anchoring groups has been designed, and the SCO characteristics of the resultant supramolecular iron(II) complexes have been investigated. By preparing a graphene−SCO complex hybrid material, we have elucidated that the interface between the molecule and graphene surface modifies the SCO parameters, relative to the parameters observed in the bulk state.[57] Subsequently, we have demonstrated spin-state dependence of conductance characteristics at a single-molecule junction composed of SLG electrodes and a pyrene-tethered iron(II)−BPP complex.[24] In another direction, we have studied transport characteristics of SCO−gold nanoparticle (Au−NP) hybrid ensembles, demonstrating the utility of iron(II)−BPP complexes featuring sulfur-based anchoring groups for the development of SCO molecule-based spintronic architectures.[47]

Despite a few studies discussed in the foregoing paragraph, the utility of iron(II)−BPP complexes as a spin-switchable entity at single-molecule junctions remains largely unexplored. In an attempt to remedy this, we have designed a set of supramolecular iron(II)−BPP complexes in view of their implementation in single SCO molecule junctions. These complexes, 1 and 2 (Scheme 1), are composed of 4-([2,2′-bithiophen]-5-ylethynyl)-2,6-di(1H-pyrazol-1-yl)pyridine (L1) and 4-(2-(5-(5-hexylthiophen-2-yl)thiophen-2-yl)ethynyl)-2,6-di(1H-pyrazol-1-yl)pyridine (L2), respectively. In the following sections, we report on the syntheses of the ligands and complexes, X-ray crystal structures of L2 and complex 2, and the SCO characteristics of complexes 1 and 2. We then present stretching-induced spin-state switching of 1 predicted by density functional theory (DFT) calculations and our attempts to study complexes 1 and 2 at a single-molecule level by connecting them between Au electrodes in a mechanically controllable break junction (MCBJ) device architecture.[58−61]

■ RESULTS AND DISCUSSION

Design and Syntheses of Ligands and Complexes. The ligands L1 and L2 feature bithiophene and hexyl-bithiophene, respectively, supramolecular functional addends tailored with the iron(II)-coordinating BPP motif via an ethynyl spacer. The ethynyl spacer between the BPP and bithiophenyl entities ensures planar ligand skeletons, which are useful for developing conductive SCO systems.[19,62−70] The presence of bithiophene groups might enable the anchoring of the complexes at single-molecule junctions. Such anchoring could be used to study the spin-state dependence of conductance at a molecular level, a progressive step toward the realization of SCO-based applications. Alkyl chain containing ligand 2 was designed to facilitate the formation of the X-ray quality of single crystals of the corresponding complex.

Ligands L1 and L2 were synthesized by performing the classical Sonogashira coupling between 4-iodo-2,6-di(1H-pyrazol-1-yl)pyridine (I-BPP)[71] and the corresponding ethynyl precursor 5-ethynyl-2,2′-bithiophene or 5-ethynyl-5′-hexyl-2,2′-bithiophene[72] as shown in Scheme 1. See Figures S1−S4 for the ¹H and ¹³C NMR spectra of the ligands. Treatment of Fe(BF₄)₂·6H₂O, dissolved in 1 mL of acetonitrile (ACN), with L1 in chloroform resulted in the formation of complex 1 as a precipitate. A similar reaction yielded a clear red-orange solution of complex 2; diffusion of diethyl ether (Et₂O) into the solution at 4 °C resulted in the formation of X-ray quality single crystals of 2.

Complex 2 crystallized with lattice acetonitrile solvents, as discussed in the section, X-ray Crystal Structures of L2 and 2. However, drying of the complex under a high vacuum resulted in the removal of cocrystallized acetonitrile solvent molecules, as inferred from thermogravimetric (Figure S5) and elemental analyses. Keeping in mind that the entire SCO investigation was done on the lattice solvent-free complex, we used the same
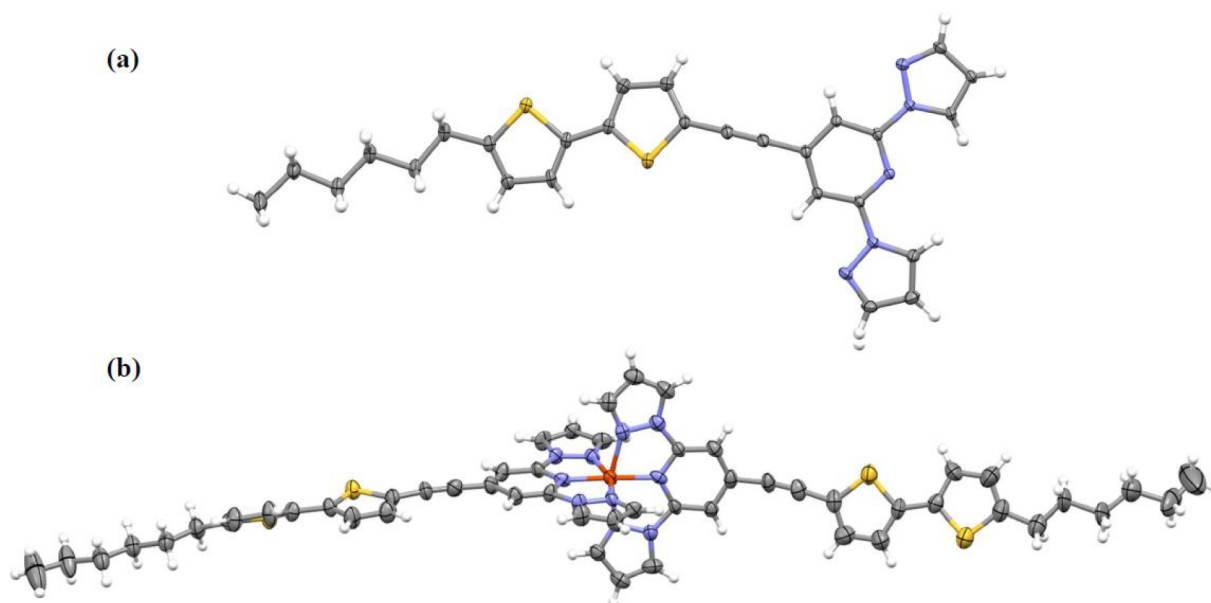
Figure 1. X-ray crystal structures of (a) **L2** and (b) complex **2**. In the case of **2**, the lattice acetonitrile solvent and counter cations are omitted for clarity. Thermal ellipsoids are drawn at 50% probability.

notation **2** for the initial and dried samples throughout the script to be more concise.

X-ray Crystal Structures of L2 and 2. X-ray structure analysis revealed the crystallization of **L2** (Figure 1a and Table S1) in the $P\bar{1}$ space group, belonging to the triclinic crystal system, with one unique molecule in the asymmetric unit. In the crystal lattice, the ligands form a one-dimensional (1D) chain along the crystallographic b axis through C−H⋯N hydrogen bond interactions between the BPP moieties (d(C10−H10⋯N1) = 2.51 Å, (∠(C10−H10⋯N1) = 174.41°), and the 1D chains are packed in the ab plane (Figure S6). In addition, the thiophene and BPP moieties stack via $\pi-\pi$ interactions along the c axis with short intermolecular contact distances of 3.32−3.40 Å.

Complex **2** crystallized (Figure 1b and Table 1) in the $P\bar{1}$ space group, belonging to the triclinic crystal system. The asymmetric unit of **2** contains a cationic $[\text{Fe}(\textbf{L2})_2]^{2+}$ unit, two BF_4^- anions, one CH_3CN molecule, and residual electron densities. The residual electron densities were flattened by employing the SQUEEZE subroutine of PLATON,[73] and the flattened electron densities (24 e$^-$ per asymmetric unit) are assigned to a disordered CH_3CN molecule (22 e$^-$), pointing to the possible presence of two additional lattice CH_3CN molecules in the unit cell. One of the peripheral hexyl chains of the $[\text{Fe}\textbf{L2}]^{2+}$ unit is disordered over two positions. The bond lengths, angles, and distortion indices, obtained using the software OctaDist,[74] of the $[\text{Fe}\textbf{L2}]^{2+}$ unit summarized in Table S2 indicate the low-spin (LS)state of the complex at 173 K, corroborating well with the LS state of the complex observed from the magnetometry study discussed in the next section.

A non-terpyridine-embrace[75] packing pattern was observed in the crystal lattice of **2**, as shown in Figure S7c. This observation is contrary to some of the BPP-based iron(II) complexes following a terpyridine-embrace packing pattern in their crystal lattice.[75,76] Six types of intermolecular interactions contribute to the packing of molecules in the crystal lattice of **2**; see the discussion in Section S4 of the Supporting Information for more details. When one considers the role of

such intermolecular noncovalent interactions in ordering of the complex entities in the crystal lattice, the complexes reported in this study are termed as supramolecular complexes.

Spin-Crossover Characteristics of 1 and 2. Variable temperature magnetometry studies were carried out to shed light on the SCO characteristics of complexes **1** and **2**. A gradual spin-state switching with $T_{1/2}$ = 254 K was observed for **1**. At 5 K, a χT value of 0.21 cm^3 mol^{-1} K was observed, indicating a LS phase contaminated with a remnant HS fraction along with a contribution from temperature independent paramagnetic (TIP) susceptibility. The TIP susceptibility arises due to the mixing of wave functions of the excited $^5\text{T}_{2g}$ state with the ground $^1\text{A}_{1g}$ state, termed as the second-order Zeeman effect.[77] Upon heating, a gradual LS-to-HS switching occurred; χT = 3.9 cm^3 mol^{-1} K obtained at 400 K, indicating the HS state of the complex at that temperature. A second heat−cool cycle (cycle 2; Figure S8) performed at a scan rate of 5 K min^{-1} yielded a similar χT versus T profile as that of cycle 1, indicating the reproducible nature of spin-state switching characteristics of **1**.

The rather high χT value obtained for the HS state of **1** compared to the one predicted on the basis of the spin only contribution (χT = 3 cm^3 mol^{-1} K) indicates the presence of significant spin−orbit coupling due to unquenched orbital angular momentum associated with the HS iron(II) center, as reported for a iron(II)−BPP complex.[78] The spin-only value is commonly used as a reference to assign the HS state of iron(II) complexes. However, such usage is not entirely correct because the $^5\text{T}_{2g}$ state features triply degenerate t$_{2g}$ orbitals with the occupancy of four (t$_{2g}^4$), giving rise to orbital angular momentum. However, in the case of LS iron(II) complexes, the t$_{2g}$ and e$_g$ orbitals are completely filled and empty, respectively; therefore, the orbital angular momentum is quenched.

For complex **2**, a χT value of 0.027 cm^3 mol^{-1} K was obtained at 5 K, indicating the LS state of the complex. The small nonzero χT values obtained for **2** below 100 K are attributed to the temperature independent paramagnetic (TIP)

susceptibility. Heating caused the onset of gradual LS-to-HS switching around 150 K, which continued until 310 K. A stepwise SCO, featuring two distinct steps with midpoints of the steps located at 313 and 321 K, followed the gradual phase. An abrupt spin-state switching ensued the stepwise region, leading to the completion of the LS-to-HS switching around 380 K. The saturated nature of the χT versus T plot and χT of 3.16 cm^3 mol^{-1} K at 400 K evidence the HS state of **2** at that temperature. Upon cooling, the HS-to-LS switching profile retraced the heating profile, except in the stepwise region, where a small hysteresis ($\Delta T_{1/2}$ = 2 K) was observed. Overall, $T_{1/2}$ of 356 K and three different types of SCO, gradual, stepwise, and abrupt, were observed for **2** in the first heat–cool cycle. The spin-state switching characteristics of **2** remained similar in the subsequent (second) heat–cool cycle (Figure S9), elucidating the stable and reproducible SCO characteristic of **2**.

To check for the role of an ordered molecular organization contributing to the occurrence of the stepwise and abrupt spin-state switching in the crystalline form of **2**, another form of the complex, hereafter referred to as complex **2a**, was prepared, and the spin-state switching characteristic of the complex was investigated. Spin-state switching of **2a** proceeded in a gradual manner without any step-like features, as shown in Figure S10. At 5 K, a χT value of 0.073 cm^3 mol^{-1} K was observed, indicating the LS state of the complex; the small χT value is attributed to the temperature independent paramagnetic susceptibility. Upon heating, a gradual LS-to-HS switching occurred; χT of 3.023 cm^3 mol^{-1} K was obtained at 400 K. Though the observed χT value is in the range expected for a HS iron(II) center (S = 2), the nonsaturation of χT versus T plot around 400 K indicates the presence of a remnant LS fraction. When the χT value of 3.16 cm^3 mol^{-1} K observed for **2** was considered as the pure HS value, a LS-to-HS conversion of ∼96% was estimated for **2a** at 400 K. Remarkably, a scan rate independent $\Delta T_{1/2}$ value of 5 K was observed for **2a** around 360 K.

Our attempts to shed light on the structural facets contributing to the occurrence of stepwise spin-state switching in complex **2** are not successful due to the cracking of the crystals above 300 K, most probably due to spontaneous lattice acetonitrile solvent loss. In the absence of experimental validations, we attribute the occurrence of stepwise SCO to temperature-dependent changes in the nearest neighbor intermolecular interactions during the switching process.[79] Such changes could have contributed to the abrupt switching of a small fraction of complexes at 313 and 321 K separated by a plateau region. The existence of such region is attributed to a thermally stable phase, albeit in a small temperature range, composed of a mixed LS/HS proportion.

Small- and Wide-Angle X-ray Scattering (SWAXS) Studies. Variable temperature SWAXS studies were performed to get insights into the molecular organization of **2** and **2a**. The SWAXS studies revealed reversible changes in the medium and wide-angle ranges of the SWAXS patterns of **2** and **2a** (Figure 3 and Figure S11) upon temperature variation, attributed to spin-state switching-induced changes in the molecular organization. A comparison between the SWAXS patterns of **2** and the simulated pattern obtained from the SCXRD study reveals that the molecular organization in **2** is different relative to the organization in the single-crystal lattice of **2**. Such difference is attributed to the absence of acetonitrile-based C–H···F and C–H···N hydrogen bonding and C–H···π

interactions in the lattice of solvent-free **2**, as against the presence of such interactions in the single-crystal lattice of **2**.

The SWAXS patterns of **2** and **2a** have quite comparable intensity profiles in the small-angle region, except for the presence of additional reflections marked with blue stars in Figure 3a,b and for small peak shifts due to slightly different lattice sizes/geometries. The comparable nature of the SWAXS profiles indicates the crystalline nature of **2a** with similar unit cell parameters as that of **2**. This also means that the molecular self-organization in the lattices of complexes **2** and **2a** is not identical but rather similar. Incidentally, the switching behavior is maintained for both complexes, although with different switching characteristics (Figures 2 and S10). This underlines
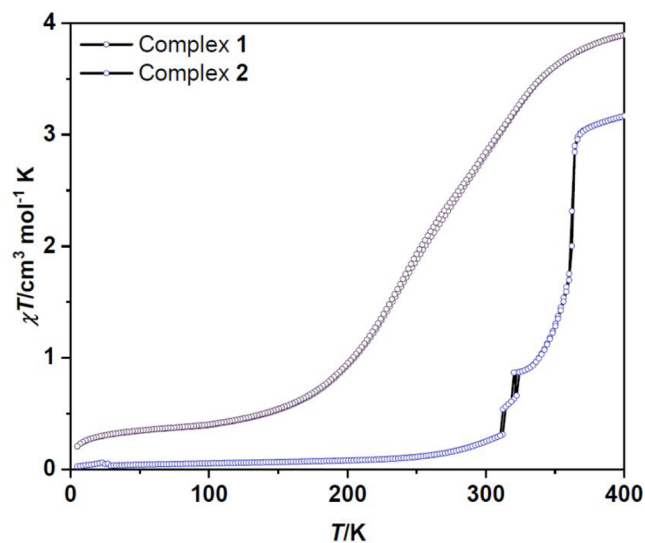

Figure 2. Spin-state switching characteristics of **1** and **2**. χT versus T plots of complexes **1** ($T_{1/2}$ = 254 K) and **2** ($T_{1/2}$ = 356 K). Experiments were performed in the settle mode under an applied DC field of 0.1 T; a scan rate of 1 K min^{-1} was employed.

that subtle changes in intermolecular interactions between **2** and **2a** can have a significant impact on the spin-state switching process. Such attribution is in line with a study by Murray and co-workers demonstrating remarkable changes in spin-state behavior associated with polymorphs of a dinuclear iron(II) complex.[77] Both SCO behaviors are nevertheless reversible, as revealed by the switchover between typical SWAXS patterns of LS and HS states and in line with the magnetometry studies.

Computational Studies: Stretching-Induced Spin-State Switching in Complex 1. The spin-state switching characteristics of complexes **1** and **2** detailed in the previous section present SCO as a macroscopic phenomenon governed by intermolecular interactions in a crystal lattice. Spin-state switching could also be induced at single-molecule junctions,[23,41] as discussed in the Introduction. In such junctions, intermolecular interactions play no role, and the switching is controlled by how a molecule interacts with an external stimulus, for example, stretching or electric field. To probe the utility of stretching as a stimulus inducing spin-state switching in iron(II)–BPP junctions, density functional theory (DFT) calculations have been performed on the basis of a model in which complex **1** is wired between Au electrodes (Figure 4a). Complex **1** is taken as a representative example, considering the similar nature of the molecular structures of **1** and **2**.
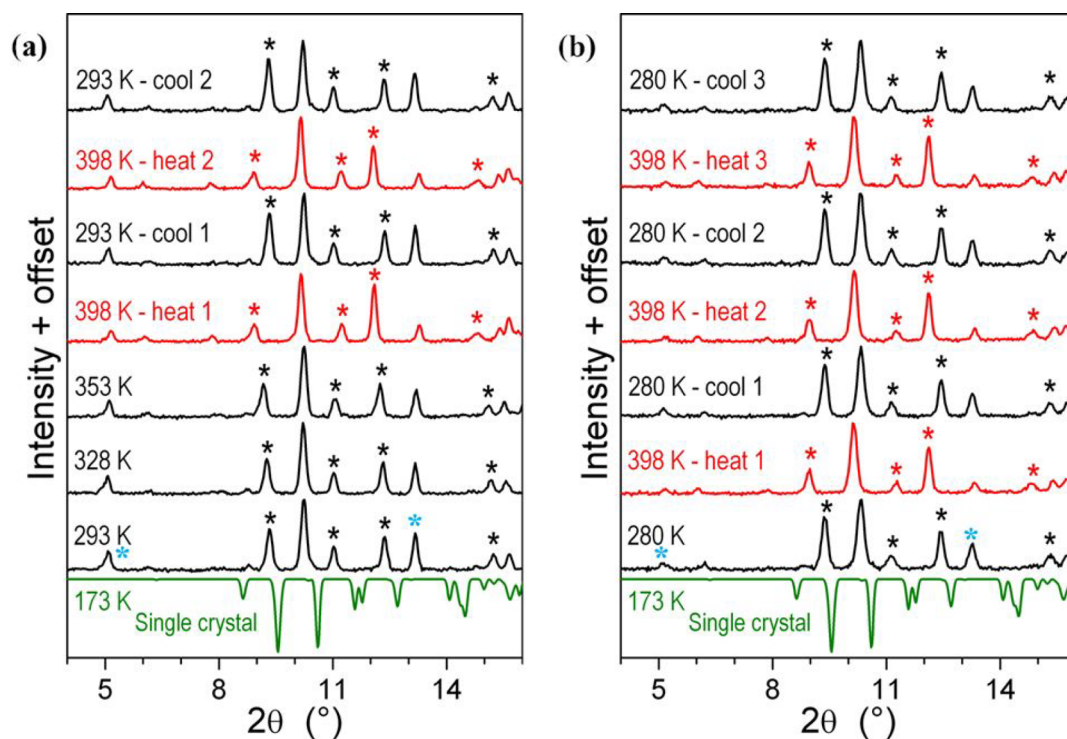
Figure 3. Variable temperature SWAXS studies. SWAXS profiles of (a) **2** and (b) **2a**. The green traces in (a) and (b) are the pattern simulated from the single-crystal X-ray structure of **2**. Blue stars mark the differences between **2** and **2a** patterns in the initial LS states. Temperature-dependent variations of the peak positions are indicated by black (LS) and red (HS) stars.
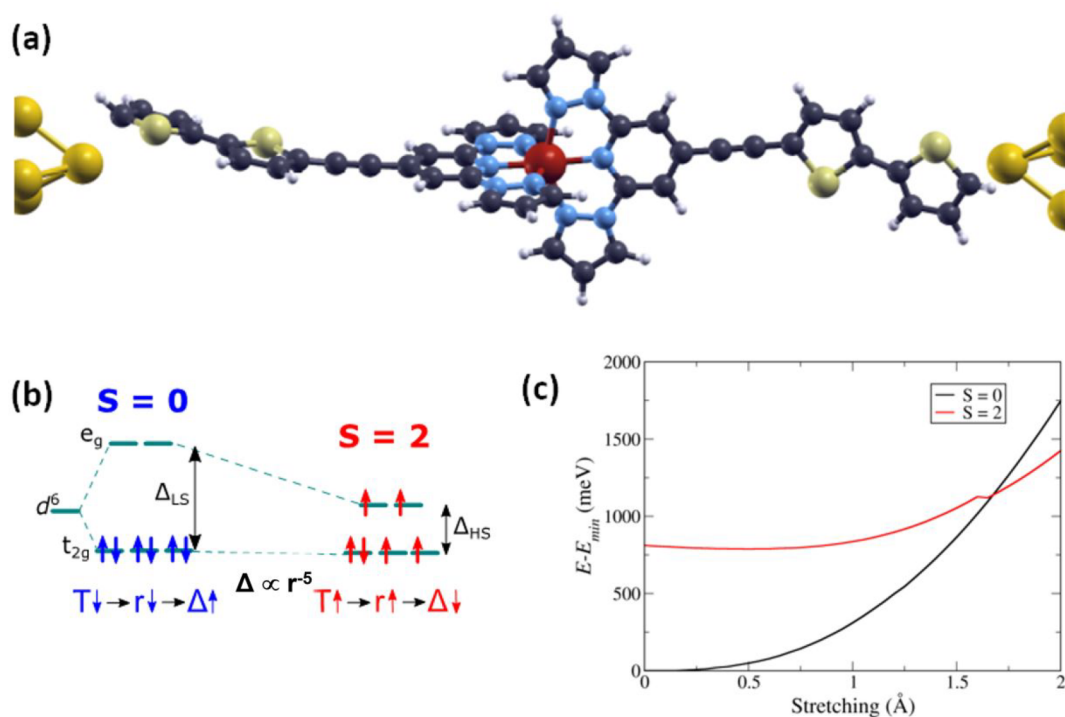

Figure 4. (a) The spin-crossover single-molecule junction, showing the molecular structure of complex **1**, and its anchoring to the pyramid apexes of the gold electrodes. (b) Mechanism of the SCO: a change in the Fe−N ligand distance r is induced by pulling the gold electrodes, which induces stretching of the compound, therefore reducing the crystal field splitting Δ. The different filling of the orbitals leads to a change in the ground state spin from $S = 0$ to $S = 2$. (c) Energy dependence $E-E_{min}$ of the two spin configurations $S = 0, 2$ of complex **1** in a vacuum, as a function of the stretching distance measured between the outermost sulfur atoms, referred to the equilibrium distance.

The ligand field interaction of approximate O_h symmetry felt by the iron(II) ion splits the 5-fold degenerate energy spectrum of its 3d electronic shell into two well-separated e_g and t_{2g} levels by a ligand field splitting energy Δ, as shown
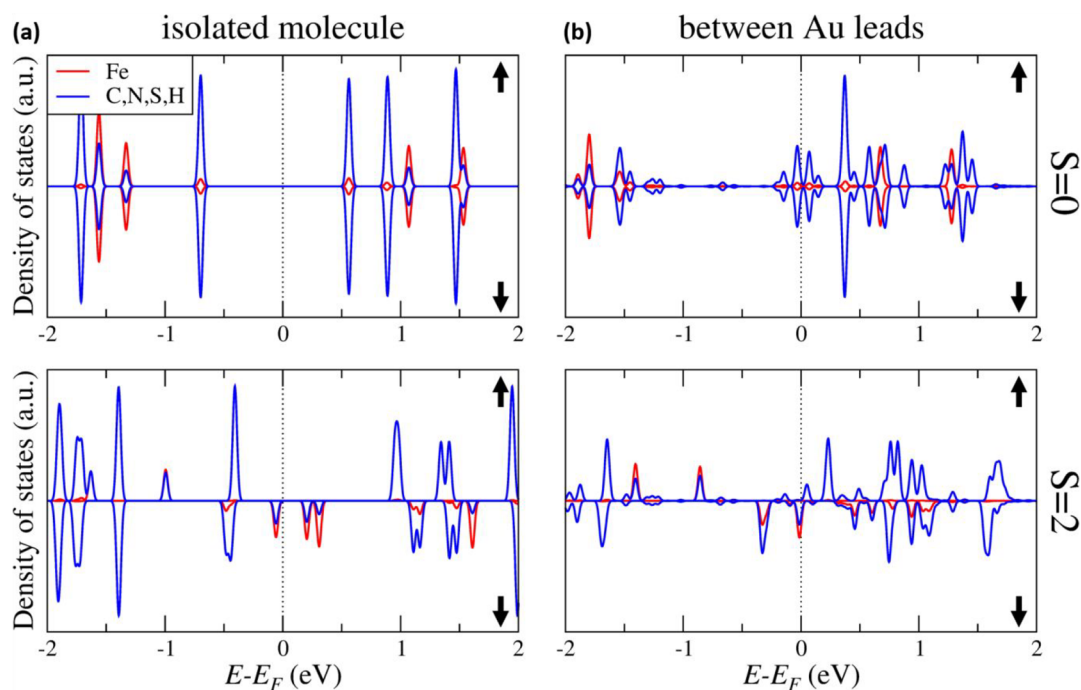
Figure 5. (a) Density of states (DOS) of isolated complex **1** in LS (top) and HS (bottom) states. (b) DOS of complex **1** anchored to the gold electrodes in LS (top) and HS (bottom) states. The DOS projected onto the iron atom and the rest of atoms in the complex are shown in red and blue lines, respectively. The black up and down arrows represent spin-up and spin-down electrons, respectively.
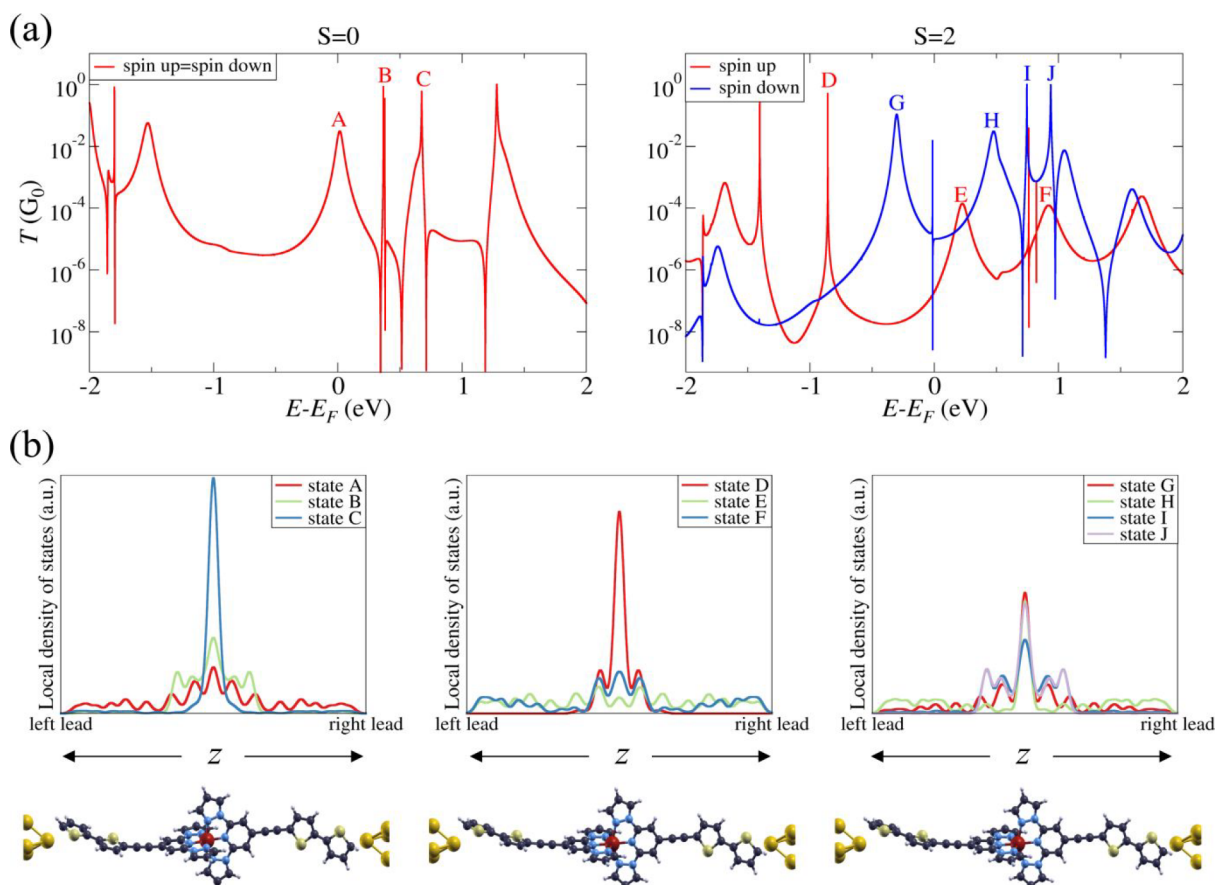
Figure 6. (a) Transmission function $T(E)$ for spin $S = 0$ (left) and $S = 2$ (right). Capital letters label transmission peaks generated by specific molecular orbitals. (b) Distribution of the density of states of each of the states labeled in (a) along an axis running longitudinally along the molecule.

Figure 7. Electrical transport properties of the junction. Current (I) versus voltage (V) characteristic of complex **1** for the (a) LS and (b) HS states. (c) Magneto-conductance ratio $I_{S=0}/I_{S=2}$ and (d) the degree of spin polarization of the current for the $S = 2$ state.
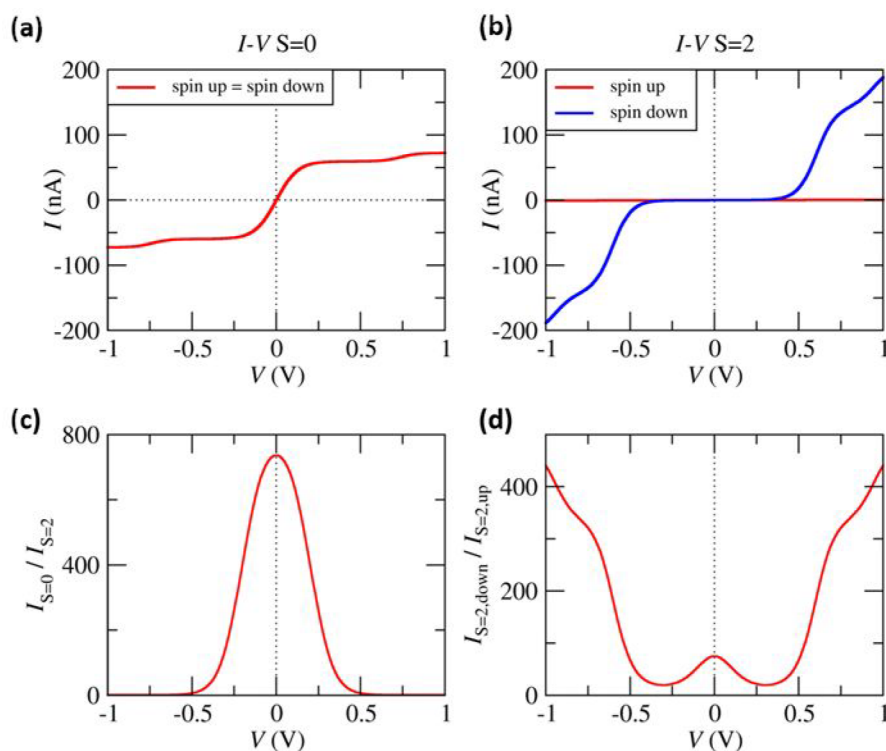
schematically in Figure 4b. The energy (Δ) depends on the average distance r between the central iron(II) ion and its neighboring ligand atoms approximately as r^{-5} and therefore is decreased by stretching it. At the equilibrium distance of the molecule, Δ is larger than the exchange interaction (pairing energy) J among the six d electrons in the iron(II) ion. As a result, complex **1** is in a low-spin (LS), $S = 0$, ground state (Figure 4b). However, Δ decreases upon stretching the molecule and becomes eventually smaller than J, making the e_g states accessible. These levels are then filled to maximize the spin multiplicity according to Hund's first principle, resulting in a high-spin (HS) state, $S = 2$, above a certain molecular length (Figure 4c). It is found from our studies that the LS–HS transition occurs when the molecule is stretched by 1.5 Å, which is about 5% greater than the initial molecular length, as shown in Figure 4c. This elongation corresponds to an increase of the Fe−N distance by about 0.15 Å, a value similar to that found for similar complexes in graphene junctions.[24] The value is also in line with about a 0.2 Å increase in Fe−N bond lengths observed for HS iron(II)−BPP complexes relative to their LS counterparts.[78,80] The calculated small bond length variation between the LS and HS states of complex **1** confirms that the spin crossover can be triggered by pulling electrodes in an MCBJ setup.

Our analyses of the electronic structure of the isolated complex **1** in LS and HS states reveal that the low-energy molecular states are mostly conjugated across the whole molecule (Figure 5a, top and bottom). Similarly, most of the low-energy molecular states of the $S = 0$ complex linked to the gold electrodes are conjugated across the whole molecule (Figure 5b, top), except for an empty state located at about +0.7 eV that has a large weight at the Fe atom. Similarly, the low-energy spin-up states of $S = 2$ of the gold-linked molecule are also conjugated across the molecule (Figure 5b, bottom),

except for an occupied state located at about −0.9 eV. In contrast, the low-energy spin-down states have all significant weight at the Fe atom. These electronic distributions have an impact on the electron transmission function across the molecule $T^S(E)$ that we depict in Figure 6. The transmission function of the $S = 0$ complex $T^0(E)$ shows a broad large-weight peak A at the Fermi energy and two narrow peaks B and C at positive energies, where only peak C corresponds to a state with a large concentration at the iron atom (Figure 6a, left). We expect that the A peak will dominate the low-voltage electrical response of the junction whenever the complex stays in the $S = 0$ state and that the impact of the B peak will be apparent at voltages larger than $V \sim 2E_B/e \sim 0.7$ V. In contrast, the $S = 2$ complex shows spin-polarized transport since $T^{2\uparrow}(E) \neq T^{2\downarrow}(E)$. The spin-up transmission function only shows the peak E at low energies and furthermore has a low transmission $T^{2\uparrow}$ of $\sim 10^{-4}$ (Figure 6a, right). In contrast, the spin-down transmission function displays two low-energy peaks G and H that have a much larger transmission $T^{2\downarrow}$ of $\sim 10^{-1}$ and are largely concentrated at the iron atom. We expect that these two peaks will give rise to a spin-down polarized current shooting up at voltages ($V \sim 2E_{G,H}/e$) of ~ 0.6 and 0.9 V, respectively.

Figure 7a shows the IV characteristics of the $S = 0$ junction. We confirm here that the junction displays a large low-voltage conductance for voltages up to about 0.25 V, which is driven by the energy location of the A peak above. In contrast, we see in Figure 7b that the $S = 2$ junction should show a very low conductance up to 0.6 V, where the down-spin peak G enters the voltage window followed by a further conductance increase at 0.9 V due to the H spin-down peak. The voltage-dependent ratio $I_{S=0}/I_{S=2}$ shown in Figure 7c quantifies this different current response. Remarkably, this ratio reaches values close to 10^3 at the lowest voltages. Figure 7d indicates that the current
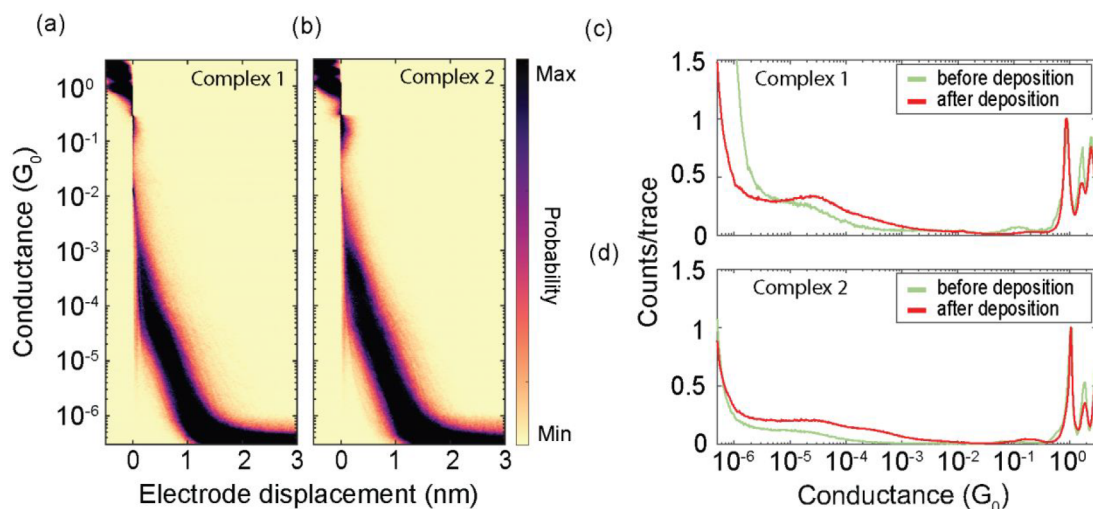
Figure 8. Two-dimensional conductance versus electrode displacement plot containing 10 000 consecutive breaking traces after deposition of (a) complex **1** and (b) complex **2**. One-dimensional conductance histograms scaled such that the conductance at $1G_0$ is fixed at 1 count/trace for (c) complex **1** and (d) complex **2**.

should show a very large degree of polarization at those voltages.

Our simulations have strong implications for MCBJ junctions. We predict that, at the initial states of a pulling cycle, the low voltage conductance should be large and spin-unpolarized. However, the low voltage conductance should show a steep drop at the threshold pulling distance even though the junction would not be broken. This should be manifested by a conductance increase around 0.6 V, where a strongly spin-polarized current is expected to set in.

Single-Molecule Transport Studies. Transport measurements were performed at room temperature using the mechanically controlled break junction (MCBJ) technique, which uses a three-point bending mechanism to break lithographically defined gold nanowires on a flexible substrate. The technique enables the user to stretch the wire until it breaks while monitoring the conductance of the junction.[81] To measure the electrical properties of the molecules, a solution containing them is drop cast onto the nanowire. The solvent evaporates, leaving the molecules on the gold surface. During breaking, the gold nanowire ultimately ruptures, and molecules can be contacted to form molecular junctions. In this way, the conductance of molecules can be monitored while separating the electrodes until the molecule loses contact. The process of stretching the junction and monitoring the conductance is called a breaking trace and can be repeated many times. In the current experiments, 0.1 mM solutions of complex **1** and **2** in dichloromethane (DCM) were used for drop-casting the molecules onto the MCBJ setup.

Figure 8a,b shows two-dimensional conductance versus electrode displacement plots displaying 10 000 consecutive breaking traces for complexes **1** and **2**, respectively. In both plots, little evidence is present of a fully stretched molecule, which would appear as a horizontal area of high counts (that is, a plateau) extending up to the length of the molecule. Figure 8c,d displays the corresponding one-dimensional conductance histograms, scaled such that at a conductance of $1G_0$ the count/trace is fixed at 1 for direct comparison. Here, G_0 is the conductance quantum, the conductance value corresponding to a single bridging gold atom. The experimental measurement of this value ensures the proper formation of an atomic

contact, which after rupture, results in two atomically sharp electrodes. In Figure 8c,d, the red curves in the conductance histograms correspond to the measurements in (a) and (b). Especially in (c), a broad peak appears around $3 \times 10^{-5} G_0$. This value corresponds to an electrode separation distance of about 0.5 nm, which is close to the lateral dimension of the complexes and can thus be indicative of the complexes perpendicularly oriented in the junction as schematically shown in for complex **1** in Figure 9. However, a laterally oriented, fully stretched molecule is the preferred choice to stretch the molecule to trigger stretching-induced spin-crossover.

Complex **1** shows gradual SCO with $T_{1/2}$ = 254 K. The fast precipitation of the complex from the reaction mixture prohibiting the orientation of the switching entities in an ordered manner could have caused the gradual SCO. The
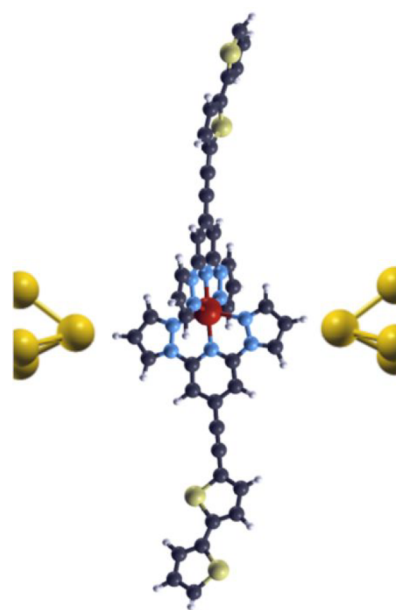

Figure 9. Tentative orientation of complex **1** in the molecular junction.

random arrangement of the molecules in the powder mitigates the effective communication of a switching event of a molecule to its nearest neighbors, thereby reducing the cooperativity. Complex **2** is one of the BPP-based complexes showing the above room temperature (RT) SCO.[76] The origin of such SCO characteristics associated with the complex is attributed to soft-intermolecular interactions operating between the switching entities. The lack of solvent molecules in the lattice of the sample used for magnetic measurement indicates the role of the intermolecular organization in governing $T_{1/2}$ and the nature of the spin-state switching process. The gradual, stepwise, and abrupt events coupled with the SCO of **2** are a testimony of complexities associated with the spin-state switching process. The absence of steps and abruptness in the spin-state switching of complex **2a**, relative to **2**, elucidates the important role of intermolecular interactions in inducing stepwise and abrupt spin-state switching and the sensitive nature of SCO even to the slightest of changes. The similar molecular organization of **2** and **2a** inferred from the SWAXS studies elucidates the role of alkyl chains facilitating molecular organization irrespective of the preparation method. Recently, we have utilized the self-assembly directing nature of the dodecyl alkyl chain to realize similar spin-state switching characteristics in the bulk and thin-film states.[82] Overall, complex **2** adds to the family of iron(II) complexes tethered with alkyl chains.[33,82−86] Such complexes show interesting structure magnetic property relationships, such as alkyl chain conformation-dependent interconversion between two distinct HS−LS states,[86] reverse SCO,[87] and tail length-dependent $T_{1/2}$.[84]

From the transport front, stretching-induced spin-state switching of iron(II)−BPP systems in single-molecule junctions is yet to be demonstrated both theoretically and experimentally to the best of our knowledge. Our attempts to experimentally demonstrate conductance switching in single-molecule junctions were not successful due to the perpendicular orientation of the complexes, instead of the fully stretched orientation, in the junctions. The DFT studies predicting the stretching-induced spin-state switching of **1** and the related spin-state-dependent conductance modulation are encouraging to develop molecular spintronic modules on the basis of the prototypical iron(II)−BPP systems.

CONCLUSIONS

The spin-state switching characteristics of supramolecular iron(II) SCO complexes, **1** and **2**, featuring organic semiconductor-like ligands **L1** and **L2** elucidate the sensitive nature of SCO to subtle changes in the molecular environment. Crucially, the SCO active nature of the complexes implies the optimal ligand field strength around iron(II) centers conducive to single-molecule transport studies aiming for the elucidation of spin-state-dependent conductance switching. Computational studies revealed that it is possible to induce SCO by stretching complex **1** in an MCBJ-like device setup. Such elucidation well augurs for the development of SCO-based spintronic elements based on the prototypical iron(II)−BPP systems. The presence of the perpendicularly oriented complexes in the junctions, instead of the expected fully stretched complexes, inferred from the single-molecule conductance traces indicates that the complexes reported in this study need to be tailored with anchoring groups with an affinity for gold electrodes to demonstrate stretching-induced spin-state switching.

METHODS

Syntheses and characterization data of the ligands and complexes discussed in this study are presented in Section S1 of the Supporting Information.

The X-ray diffraction data collection of the ligand **L2** was carried out on a Bruker PHOTON-III CPAD diffractometer using Mo Kα radiation (λ = 0.71073 Å) under a cold nitrogen stream at 120 K. The X-ray diffraction data collection of the complex **2** was carried out on a Bruker APEX II DUO Kappa-CCD diffractometer using Cu Kα radiation (λ = 1.54178 Å) under a cold nitrogen stream at 173 K. The cell refinement and data reduction were performed using SAINT in APEX3 (APEX3: SAINT-Plus and SADABS, Bruker AXS Inc., Madison, Wisconsin, USA, 2016). A semiempirical absorption correction was applied using SADABS in APEX3. The structures were solved by direct methods (SHELXT Version 2014/5)[88] and standard difference map techniques and refined using full-matrix least-squares procedures on F_2. The refinement and all further calculations were carried out using SHELXL Version 2014/7.[89] Anisotropic refinement was applied to all non-hydrogen atoms. All hydrogen atoms were placed at the calculated positions and refined using a riding model. The residual electron densities corresponding to the disordered solvents in complex **2** were flattened by employing the SQUEEZE subroutine of PLATON.[73] One of the peripheral hexyl chains of the $[\text{Fe}(\textbf{L2})_2]^{2+}$ unit in complex **2** was refined over two positions with constraints on the temperature parameters (EADP commands).

Magnetic measurements were performed on a MPMS-3 SQUID-VSM magnetometer (Quantum Design). The temperature-dependent magnetization was recorded at an applied DC field of 0.1 T. Temperature sweeping rates of 5 and 1 K min^{-1} were employed. Gelatin capsules were used as sample holders in the 5 to 400 K temperature range.

Small- and wide-angle X-ray scattering (SWAXS) patterns were obtained with a linear monochromatic Cu Kα1 beam (λ = 1.5405 Å). The beam was obtained using a sealed-tube generator equipped with a bent quartz monochromator and a curved Inel CPS 120 counter gas-filled detector. Periodicities of up to 70 Å can be measured, and the sample temperature was controlled to within ±0.01 °C from 5 to 200 °C. The sample was filled in sealed cells of adjustable paths, and the exposure time was 4 h.

SIMULATIONS

We have used the *ab initio* code SIESTA[90] to extract the properties of the single-molecule complex **1** discussed in the body of the manuscript. Simulations were performed for complex **1** in vacuum as well as for a full junction, where complex **1** was linked to gold electrodes. We used a double-ζ polarized basis set for all atoms in the simulation having radii on the order of 7 Bohr or larger. We also used fully tested pseudopotentials for all atomic species in the simulations. We used the conventional exchange-correlation GGA-PBE functional.[91]

Simulations of the whole junction were carried out so that each gold electrode was oriented along the (111) crystallographic direction. Each electrode was then terminated by a four atomic layer pyramid having atom numbers of 10−6−3−1. Complex **1** was then inserted in the junction. Simulations were performed for a range of distances between the pyramid tips of the two electrodes. The complex was allowed to relax

for each distance (d) until the largest atomic force was smaller than 0.02 eV/angstrom, and then, we extracted the total energy of the junction, $E^S(d)$. The final junction arrangement was chosen at the tip−tip distance (d_0) that yielded the lowest energy. We found that $E^{S=0}(d_0) < E^{S=2}(d_0)$ as expected.

All transport calculations were performed with the GOLLUM package,[92] where the junction Hamiltonians were read from SIESTA's output at the equilibrium tip distance, d_0.

■ ASSOCIATED CONTENT

ⓢ Supporting Information

The Supporting Information is available free of charge at https://pubs.acs.org/doi/10.1021/acsomega.1c07217.

> Procedures used to synthesize ligands and complexes, ^1H and ^{13}C NMR spectra of the ligands in CD_2Cl_2, thermogravimetric analyses of complexes **2** and **2a**, analyses of X-ray crystal structures of **L2** and complex **2**, magnetometry studies of **1** and **2** performed at a scan rate of 5 K min^{-1}, and small- and wide-angle X-ray scattering (SWAXS) studies of complexes **2** and **2a** (PDF)

■ AUTHOR INFORMATION

Corresponding Authors

Senthil Kumar Kuppusamy − *Institute for Quantum Materials and Technologies (IQMT), Karlsruhe Institute of Technology (KIT), 76344 Eggenstein-Leopoldshafen, Germany;* ⓞ orcid.org/0000-0002-1501-7759; Email: senthil.kuppusamy2@kit.edu

Jaime Ferrer − *Departamento de Física, Universidad de Oviedo, ES-33007 Oviedo, Spain; Centro de Investigación en Nanotecnología y Nanomateriales (CINN, CSIC), El Entrego ES-33940, Spain;* Email: ferrer@uniovi.es

Herre S. J. van der Zant − *Kavli Institute of Nanoscience, Delft University of Technology, 2600 GA Delft, The Netherlands;* ⓞ orcid.org/0000-0002-5385-0282; Email: H.S.J.vanderZant@tudelft.nl

Mario Ruben − *Institute for Quantum Materials and Technologies (IQMT), Karlsruhe Institute of Technology (KIT), 76344 Eggenstein-Leopoldshafen, Germany; Institute of Nanotechnology, Karlsruhe Institute of Technology (KIT), 76344 Eggenstein-Leopoldshafen, Germany; Université de Strasbourg (Unistra), Institute de Science et d'Ingénierie Supramoléculaire (ISIS), Centre Européen de Science Quantique (CESQ), F-67000 Strasbourg, France;* Email: mario.ruben@kit.edu

Authors

Asato Mizuno − *Institute of Nanotechnology, Karlsruhe Institute of Technology (KIT), 76344 Eggenstein-Leopoldshafen, Germany; Present Address: Department of Life and Coordination-Complex Molecular Science, Institute for Molecular Science, 5-1 Higashiyama, Myodaiji, Okazaki, Aichi 444-8787, Japan*

Amador García-Fuente − *Departamento de Física, Universidad de Oviedo, ES-33007 Oviedo, Spain; Centro de Investigación en Nanotecnología y Nanomateriales (CINN, CSIC), El Entrego ES-33940, Spain;* ⓞ orcid.org/0000-0002-4570-8315

Sebastiaan van der Poel − *Kavli Institute of Nanoscience, Delft University of Technology, 2600 GA Delft, The Netherlands*

Benoît Heinrich − *Institut de Physique et Chimie des Matériaux de Strasbourg (IPCMS), 67034 cedex 2 Strasbourg, France;* ⓞ orcid.org/0000-0001-6795-2733

Complete contact information is available at: https://pubs.acs.org/10.1021/acsomega.1c07217

Notes

The authors declare no competing financial interest.

■ ACKNOWLEDGMENTS

■ REFERENCES

(1) Deorukhkar, N.; Besnard, C.; Guénée, L.; Piguet, C. Tuning spin-srossover transition temperatures in non-symmetrical homoleptic meridional/facial [Fe(Didentate)$_3$]$^{2+}$ complexes: what for and who cares about it? *Dalton Trans* **2021**, *50*, 1206−1223.

(2) Koenig, E.; Madeja, K. 5T2−1A1 Equilibriums in some iron(II)-bis(1,10-phenanthroline) complexes. *Inorg. Chem.* **1967**, *6* (1), 48−55.

(3) Gütlich, P.; Hauser, A.; Spiering, H. Thermal and Optical Switching of Iron(II) Complexes. *Angew. Chem., Int. Ed. Engl.* **1994**, *33* (20), 2024−2054.

(4) Halcrow, M. A., Ed. *Spin-Crossover Materials: Properties and Applications*; John Wiley & Sons Ltd.: Oxford, UK, 2013; DOI: 10.1002/9781118519301.

(5) Goodwin, H. A. Spin Transitions in six-coordinate iron(II) complexes. *Coord. Chem. Rev.* **1976**, *18* (3), 293−325.

(6) Baker, W. A.; Bobonich, H. M. Magnetic Properties of Some High-Spin Complexes of Iron(II). *Inorg. Chem.* **1964**, *3* (8), 1184−1188.

(7) Brooker, S. Spin crossover with thermal hysteresis: practicalities and lessons learnt. *Chem. Soc. Rev.* **2015**, *44* (10), 2880−2892.

(8) Kahn, O.; Martinez, C. J. Spin-Transition Polymers: From Molecular Materials Toward Memory Devices. *Science* **1998**, *279* (5347), 44−48.

(9) Senthil Kumar, K.; Ruben, M. Emerging trends in spin crossover (SCO) based functional materials and devices. *Coord. Chem. Rev.* **2017**, *346*, 176−205.

(10) Kumar, K. S.; Ruben, M. Sublimable Spin-Crossover Complexes: From Spin-State Switching to Molecular Devices. *Angew. Chem. Int. Ed* **2021**, *60* (14), 7502−7521.

(11) Halcrow, M. A. Manipulating metal spin states for biomimetic, catalytic and molecular materials chemistry. *Dalton Trans* **2020**, *49* (44), 15560−15567.

(12) Gütlich, P.; Goodwin, H. A., Eds. *Spin Crossover in Transition Metal Compounds*; Topics in Current Chemistry; Springer: Berlin, New York, 2004.

(13) Weber, B.; Bauer, W.; Obel, J. An Iron(II) Spin-Crossover Complex with a 70 K Wide Thermal Hysteresis Loop. *Angew. Chem. Int. Ed* **2008**, *47* (52), 10098−10101.

(14) Goodwin, H. A. Spin Crossover in Cobalt(II) Systems. In *Spin Crossover in Transition Metal Compounds II*; Topics in Current Chemistry; Springer Berlin Heidelberg: Berlin, Heidelberg, 2004; Vol. *234*, pp 23−47; DOI: 10.1007/b95411.

(15) Krivokapic, I.; Zerara, M.; Daku, M. L.; Vargas, A.; Enachescu, C.; Ambrus, C.; Tregenna-Piggott, P.; Amstutz, N.; Krausz, E.; Hauser, A. Spin-crossover in cobalt(II) imine complexes. *Coord. Chem. Rev.* **2007**, *251* (3−4), 364−378.

(16) Wang, S.; Li, Y.-J.; Ju, F.-F.; Xu, W.-T.; Kagesawa, K.; Li, Y.-H.; Yamashita, M.; Huang, W. The molecular and supramolecular aspects in mononuclear manganese(III) Schiff-base spin crossover complexes. *Dalton Trans* **2017**, *46* (33), 11063−11077.

(17) Garcia, Y.; Gütlich, P. Thermal Spin Crossover in Mn(II), Mn(III), Cr(II) and Co(III) Coordination Compounds. In *Spin Crossover in Transition Metal Compounds II*; Topics in Current Chemistry; Springer Berlin Heidelberg: Berlin, Heidelberg, 2004; Vol. *234*, pp 49−62; DOI: 10.1007/b95412.

(18) Morgan, G. G.; Murnaghan, K. D.; Müller-Bunz, H.; McKee, V.; Harding, C. J. A Manganese(III) Complex That Exhibits Spin Crossover Triggered by Geometric Tuning. *Angew. Chem. Int. Ed* **2006**, *45* (43), 7192−7195.

(19) Kazakova, A. V.; Tiunova, A. V.; Korchagin, D. V.; Shilov, G. V.; Yagubskii, E. B.; Zverev, V. N.; Yang, S. C.; Lin, J.; Lee, J.; Maximova, O. V.; Vasiliev, A. N. The First Conducting Spin-Crossover Compound Combining a Mn^III Cation Complex with Electroactive TCNQ Demonstrating an Abrupt Spin Transition with a Hysteresis of 50 K. *Chem. − Eur. J.* **2019**, *25* (43), 10204−10213.

(20) Gütlich, P.; Garcia, Y. Spin Crossover Systems. In *Reference Module in Chemistry, Molecular Sciences and Chemical Engineering*; Elsevier, 2015; DOI: 10.1016/B978-0-12-409547-2.11373-3.

(21) Halcrow, M. A. Spin-Crossover Compounds with Wide Thermal Hysteresis. *Chem. Lett.* **2014**, *43* (8), 1178−1188.

(22) Sanvito, S. Molecular spintronics. *Chem. Soc. Rev.* **2011**, *40* (6), 3336.

(23) Miyamachi, T.; Gruber, M.; Davesne, V.; Bowen, M.; Boukari, S.; Joly, L.; Scheurer, F.; Rogez, G.; Yamada, T. K.; Ohresser, P.; Beaurepaire, E.; Wulfhekel, W. Robust spin crossover and memristance across a single molecule. *Nat. Commun.* **2012**, *3* (1), 938.

(24) Burzurí, E.; García-Fuente, A.; García-Suárez, V.; Senthil Kumar, K.; Ruben, M.; Ferrer, J.; van der Zant, H. S. J. Spin-state dependent conductance switching in single molecule-graphene junctions. *Nanoscale* **2018**, *10* (17), 7905−7911.

(25) Ke, G.; Duan, C.; Huang, F.; Guo, X. Electrical and spin switches in single-molecule junctions. *InfoMat* **2020**, *2* (1), 92−112.

(26) Wagner, S.; Kisslinger, F.; Ballmann, S.; Schramm, F.; Chandrasekar, R.; Bodenstein, T.; Fuhr, O.; Secker, D.; Fink, K.; Ruben, M.; Weber, H. B. Switching of a coupled spin pair in a single-molecule junction. *Nat. Nanotechnol* **2013**, *8* (8), 575−579.

(27) Li, J.; Wu, Q.; Xu, W.; Wang, H.-C.; Zhang, H.; Chen, Y.; Tang, Y.; Hou, S.; Lambert, C. J.; Hong, W. Room-Temperature Single-Molecule Conductance Switch via Confined Coordination-Induced Spin-State Manipulation. *CCS Chem.* **2021**, 1744−1752.

(28) Aragonès, A. C.; Aravena, D.; Cerdá, J. I.; Acís-Castillo, Z.; Li, H.; Real, J. A.; Sanz, F.; Hihath, J.; Ruiz, E.; Díez-Pérez, I. Large Conductance Switching in a Single-Molecule Device through Room Temperature Spin-Dependent Transport. *Nano Lett.* **2016**, *16* (1), 218−226.

(29) Ormaza, M.; Abufager, P.; Verlhac, B.; Bachellier, N.; Bocquet, M.-L.; Lorente, N.; Limot, L. Controlled spin switching in a metallocene molecular junction. *Nat. Commun.* **2017**, *8* (1), 1974.

(30) Parks, J. J.; Champagne, A. R.; Costi, T. A.; Shum, W. W.; Pasupathy, A. N.; Neuscamman, E.; Flores-Torres, S.; Cornaglia, P. S.; Aligia, A. A.; Balseiro, C. A.; Chan, G. K.-L.; Abruña, H. D.; Ralph, D. C. Mechanical Control of Spin States in Spin-1 Molecules and the Underscreened Kondo Effect. *Science* **2010**, *328* (5984), 1370−1373.

(31) Real, J. A.; Gaspar, A. B.; Niel, V.; Muñoz, M. C. Communication between iron(II) building blocks in cooperative spin transition phenomena. *Coord. Chem. Rev.* **2003**, *236* (1−2), 121−141.

(32) Guionneau, P.; Létard, J.-F.; Yufit, D. S.; Chasseau, D.; Bravic, G.; Goeta, A. E.; Howard, J. A. K.; Kahn, O. Structural approach of the features of the spin crossover transition in iron (II) compounds. *J. Mater. Chem.* **1999**, *9* (4), 985−994.

(33) Schlamp, S.; Weber, B.; Naik, A. D.; Garcia, Y. Cooperative spin transition in a lipid layer like system. *Chem. Commun.* **2011**, *47* (25), 7152.

(34) Komatsu, Y.; Kato, K.; Yamamoto, Y.; Kamihata, H.; Lee, Y. H.; Fuyuhiro, A.; Kawata, S.; Hayami, S. Spin-Crossover Behaviors Based on Intermolecular Interactions for Cobalt(II) Complexes with Long Alkyl Chains. *Eur. J. Inorg. Chem.* **2012**, *2012* (16), 2769−2775.

(35) Seredyuk, M.; Znovjyak, K.; Valverde-Muñoz, F. J.; Muñoz, M. C.; Fritsky, I. O.; Amirkhanov, V. M.; Real, J. A. Spin transition and symmetry-breaking in new mononuclear Fe^II tren-complexes with up to 38 K hysteresis around room temperature. *Inorg. Chem. Front* **2022**, *9*, 537−546.

(36) Vela, S.; Paulsen, H. Cooperativity in Spin Crossover Systems. An Atomistic Perspective on the Devil's Staircase. *Inorg. Chem.* **2018**, *57* (15), 9478−9488.

(37) Meded, V.; Bagrets, A.; Fink, K.; Chandrasekar, R.; Ruben, M.; Evers, F.; Bernand-Mantel, A.; Seldenthuis, J. S.; Beukman, A.; van der Zant, H. S. J. Electrical control over the Fe(II) spin crossover in a single molecule: Theory and Experiment. *Phys. Rev. B* **2011**, *83* (24), 245415.

(38) Harzmann, G. D.; Frisenda, R.; van der Zant, H. S. J.; Mayor, M. Single-Molecule Spin Switch Based on Voltage-Triggered Distortion of the Coordination Sphere. *Angew. Chem. Int. Ed* **2015**, *54* (45), 13425−13430.

(39) Frisenda, R.; Harzmann, G. D.; Celis Gil, J. A.; Thijssen, J. M.; Mayor, M.; van der Zant, H. S. J. Stretching-Induced Conductance Increase in a Spin-Crossover Molecule. *Nano Lett.* **2016**, *16* (8), 4733−4737.

(40) Johannsen, S.; Ossinger, S.; Markussen, T.; Tuczek, F.; Gruber, M.; Berndt, R. Electron-Induced Spin-Crossover in Self-Assembled Tetramers. *ACS Nano* **2021**, *15* (7), 11770−11778.

(41) Gopakumar, T. G.; Matino, F.; Naggert, H.; Bannwarth, A.; Tuczek, F.; Berndt, R. Electron-Induced Spin Crossover of Single Molecules in a Bilayer on Gold. *Angew. Chem. Int. Ed* **2012**, *51* (25), 6262−6266.

(42) Boudalis, A. K.; Kumar, K. S.; Ruben, M. Molecular Devices. In *Comprehensive Coordination Chemistry III*; Elsevier, 2021; pp 206−240; DOI: 10.1016/B978-0-08-102688-5.00061-1.

(43) Hao, H.; Jia, T.; Zheng, X.; Liu, P.; Zeng, Z. One-electron reduction induced spin transition in Fe(II) spin crossover molecules and the effect of the ligand. *J. Mater. Chem. C* **2021**, *9* (14), 4808−4814.

(44) Hao, H.; Jia, T.; Zheng, X.; Liu, P.; Zeng, Z. Bias induced spin state transition mediated by electron excitations. *J. Chem. Phys.* **2020**, *152* (13), 134301.

(45) Ruiz, E. Charge transport properties of spin crossover systems. *Phys. Chem. Chem. Phys.* **2014**, *16* (1), 14−22.

(46) Aravena, D.; Ruiz, E. Coherent Transport through Spin-Crossover Single Molecules. *J. Am. Chem. Soc.* **2012**, *134* (2), 777−779.

(47) Devid, E. J.; Martinho, P. N.; Kamalakar, M. V.; Šalitroš, I.; Prendergast, Ú.; Dayen, J.-F.; Meded, V.; Lemma, T.; González-Prieto, R.; Evers, F.; Keyes, T. E.; Ruben, M.; Doudin, B.; van der Molen, S. J. Spin Transition in Arrays of Gold Nanoparticles and Spin Crossover Molecules. *ACS Nano* **2015**, *9* (4), 4496−4507.

(48) Halcrow, M. A. Iron(II) complexes of 2,6-di(pyrazol-1-Yl)pyridines—A versatile system for spin-crossover research. *Coord. Chem. Rev.* **2009**, *253* (21−22), 2493−2514.

(49) Senthil Kumar, K.; Del Giudice, N.; Heinrich, B.; Douce, L.; Ruben, M. Bistable spin-crossover in a new series of [Fe(BPP-R)₂]^{2+} (BPP = 2,6-bis(pyrazol-1-Yl)pyridine; R = CN) complexes. *Dalton Trans* **2020**, *49* (40), 14258−14267.

(50) Senthil Kumar, K.; Heinrich, B.; Vela, S.; Moreno-Pineda, E.; Bailly, C.; Ruben, M. Bi-stable spin-crossover characteristics of a highly distorted [Fe(1-BPP-COOC₂H₅)₂](ClO₄)₂·CH₃CN complex. *Dalton Trans* **2019**, *48* (12), 3825−3830.

(51) Halcrow, M. A. Recent advances in the synthesis and applications of 2,6-dipyrazolylpyridine derivatives and their complexes. *New J. Chem.* **2014**, *38* (5), 1868−1882.

(52) Kumar, K. S.; Šalitroš, I.; Moreno-Pineda, E.; Ruben, M. Spacer type mediated tunable spin crossover (SCO) characteristics of pyrene

decorated 2,6-bis(pyrazol-1-Yl)pyridine (bpp) based Fe(II) molecular spintronic modules. *Dalton Trans* **2017**, *46* (30), 9765−9768.

(53) Kumar, K. S.; Šalitroš, I.; Suryadevara, N.; Moreno-Pineda, E.; Ruben, M. Supramolecular Interaction Tuning of Spin-Crossover in Pyrene/Fullerene (C$_{60}$) Tethered Fe^{II}-2,6-Di(Pyrazol-1-Yl)Pyridine Complexes: Towards Switchable Molecular Devices. *Eur. J. Inorg. Chem.* **2018**, *2018* (47), 5091−5097.

(54) González-Prieto, R.; Fleury, B.; Schramm, F.; Zoppellaro, G.; Chandrasekar, R.; Fuhr, O.; Lebedkin, S.; Kappes, M.; Ruben, M. Tuning the spin-transition properties of pyrene-decorated 2,6-bispyrazolylpyridine based Fe(II) complexes. *Dalton Trans* **2011**, *40* (29), 7564−7570.

(55) Nuin, E.; Bauer, W.; Hirsch, A. Synthesis of Magnetic Molecular Complexes with Fullerene Anchor Groups: Synthesis of Magnetic Molecular Complexes with Fullerene Anchor Groups. *Eur. J. Org. Chem.* **2017**, *2017* (4), 790−798.

(56) Palacios-Corella, M.; Ramos-Soriano, J.; Souto, M.; Ananias, D.; Calbo, J.; Ortí, E.; Illescas, B. M.; Clemente-León, M.; Martín, N.; Coronado, E. Hexakis-adducts of [60]fullerene as molecular scaffolds of polynuclear spin-crossover molecules. *Chem. Sci.* **2021**, *12*, 757.

(57) Senthil Kumar, K.; Šalitroš, I.; Boubegtiten-Fezoua, Z.; Moldovan, S.; Hellwig, P.; Ruben, M. A Spin crossover (SCO) active graphene-iron(II) complex hybrid material. *Dalton Trans* **2018**, *47* (1), 35−40.

(58) Xiang, D.; Jeong, H.; Lee, T.; Mayer, D. Mechanically Controllable Break Junctions for Molecular Electronics. *Adv. Mater.* **2013**, *25* (35), 4845−4867.

(59) Wang, L.; Wang, L.; Zhang, L.; Xiang, D. Advance of Mechanically Controllable Break Junction for Molecular Electronics. *Top. Curr. Chem.* **2017**, *375* (3), 61.

(60) Schwarz, F.; Lörtscher, E. Break-junctions for investigating transport at the molecular scale. *J. Phys.: Condens. Matter* **2014**, *26* (47), 474201.

(61) Gehring, P.; Thijssen, J. M.; van der Zant, H. S. J. Single-molecule quantum-transport phenomena in break junctions. *Nat. Rev. Phys.* **2019**, *1* (6), 381−396.

(62) Nihei, M.; Takahashi, N.; Nishikawa, H.; Oshio, H. Spin-crossover behavior and electrical conduction property in iron(II) complexes with tetrathiafulvalene moieties. *Dalton Trans* **2011**, *40* (10), 2154−2156.

(63) Coronado, E.; Galán-Mascarós, J. R.; Gómez-García, C. J.; Laukhin, V. Coexistence of ferromagnetism and metallic conductivity in a molecule-based layered compound. *Nature* **2000**, *408* (6811), 447−449.

(64) Rubio-Giménez, V.; Tatay, S.; Martí-Gastaldo, C. Electrical conductivity and magnetic bistability in metal−organic frameworks and coordination polymers: charge transport and cpin crossover at the nanoscale. *Chem. Soc. Rev.* **2020**, *49* (15), 5601−5638.

(65) Faulmann, C.; Jacob, K.; Dorbes, S.; Lampert, S.; Malfant, I.; Doublet, M.-L.; Valade, L.; Real, J. A. Electrical Conductivity and Spin Crossover: A New Achievement with a Metal Bis Dithiolene Complex. *Inorg. Chem.* **2007**, *46* (21), 8548−8559.

(66) Phan, H.; Benjamin, S. M.; Steven, E.; Brooks, J. S.; Shatruk, M. Photomagnetic Response in Highly Conductive Iron(II) Spin-Crossover Complexes with TCNQ Radicals. *Angew. Chem. Int. Ed* **2015**, *54* (3), 823−827.

(67) Djukic, B.; Lemaire, M. T. Hybrid Spin-Crossover Conductor Exhibiting Unusual Variable-Temperature Electrical Conductivity. *Inorg. Chem.* **2009**, *48* (22), 10489−10491.

(68) Djukic, B.; Dube, P. A.; Razavi, F.; Seda, T.; Jenkins, H. A.; Britten, J. F.; Lemaire, M. T. Preparation and Magnetic Properties of Iron(3+) Spin-Crossover Complexes Bearing a Thiophene Substituent: Toward Multifunctional Metallopolymers. *Inorg. Chem.* **2009**, *48* (2), 699−707.

(69) Ishikawa, R.; Ueno, S.; Nifuku, S.; Horii, Y.; Iguchi, H.; Miyazaki, Y.; Nakano, M.; Hayami, S.; Kumagai, S.; Katoh, K.; Li, Z.; Yamashita, M.; Kawata, S. Simultaneous Spin-Crossover Transition and Conductivity Switching in a Dinuclear Iron(II) Coordination Compound Based on 7,7′,8,8′-Tetracyano- *p* -quinodimethane. *Chem. − Eur. J.* **2020**, *26* (6), 1278−1285.

(70) Üngör, Ö.; Shatruk, M. Transition metal complexes with fractionally charged TCNQ radical anions as structural templates for multifunctional molecular conductors. *Polyhedron* **2020**, *177*, 114254.

(71) Rajadurai, C.; Schramm, F.; Brink, S.; Fuhr, O.; Ghafari, M.; Kruk, R.; Ruben, M. Spin Transition in a Chainlike Supramolecular Iron(II) Complex. *Inorg. Chem.* **2006**, *45* (25), 10019−10021.

(72) Meng, Q.; Gao, J.; Li, R.; Jiang, L.; Wang, C.; Zhao, H.; Liu, C.; Li, H.; Hu, W. New type of organic semiconductors for field-effect transistors with carbon-carbon triple bonds. *J. Mater. Chem.* **2009**, *19* (10), 1477.

(73) Spek, A. L. *PLATON* SQUEEZE: a tool for the calculation of the disordered solvent contribution to the calculated structure factors. *Acta Crystallogr. Sect. C Struct. Chem.* **2015**, *71* (1), 9−18.

(74) Ketkaew, R.; Tantirungrotechai, Y.; Harding, P.; Chastanet, G.; Guionneau, P.; Marchivie, M.; Harding, D. J. OctaDist: a tool for calculating distortion parameters in spin crossover and coordination complexes. *Dalton Trans* **2021**, *50*, 1086−1096.

(75) Pritchard, R.; Kilner, C. A.; Halcrow, M. A. Iron(II) complexes with a terpyridine embrace packing motif show remarkably consistent cooperative spin-transitions. *Chem. Commun.* **2007**, 577−579.

(76) Halcrow, M. A.; Capel Berdiell, I.; Pask, C. M.; Kulmaczewski, R. Relationship between the Molecular Structure and Switching Temperature in a Library of Spin-Crossover Molecular Materials. *Inorg. Chem.* **2019**, *58* (15), 9811−9821.

(77) Schneider, C. J.; Cashion, J. D.; Chilton, N. F.; Etrillard, C.; Fuentealba, M.; Howard, J. A. K.; Létard, J.; Milsmann, C.; Moubaraki, B.; Sparkes, H. A.; Batten, S. R.; Murray, K. S. Spin Crossover in a 3,5-Bis(2-pyridyl)-1,2,4-triazolate-Bridged Dinuclear Iron(II) Complex [{Fe(NCBH$_3$)(Py)}$_2$(μ-L^1)$_2$] − Powder versus Single Crystal Study. *Eur. J. Inorg. Chem.* **2013**, *2013* (5−6), 850−864.

(78) Hasegawa, Y.; Sakamoto, R.; Takahashi, K.; Nishihara, H. Bis[(*E*)-2,6-Bis(1*H*-Pyrazol-1-Yl)-4-Styrylpyridine]Iron(II) Complex: Relationship between Thermal Spin Crossover and Crystal Solvent. *Inorg. Chem.* **2013**, *52* (3), 1658−1665.

(79) Kilner, C. A.; Halcrow, M. A. An unusual discontinuity in the thermal spin transition in [Co(Terpy)$_2$][BF$_4$]$_2$. *Dalton Trans* **2010**, *39* (38), 9008−9012.

(80) Suryadevara, N.; Mizuno, A.; Spieker, L.; Salamon, S.; Sleziona, S.; Maas, A.; Pollmann, E.; Heinrich, B.; Schleberger, M.; Wende, H.; Kuppusamy, S. K.; Ruben, M. Structural Insights into Hysteretic Spin-Crossover in a Set of Iron(II)-2,6-bis(1 *H* -Pyrazol-1-yl)Pyridine) Complexes. *Chem. − Eur. J.* **2022**, *28* (6), e202103853.

(81) Martin, C. A.; Smit, R. H. M.; van Egmond, R.; van der Zant, H. S. J.; van Ruitenbeek, J. M. A versatile low-temperature setup for the electrical characterization of single-molecule junctions. *Rev. Sci. Instrum.* **2011**, *82* (5), 053907.

(82) Kumar, K. S.; Studniarek, M.; Heinrich, B.; Arabski, J.; Schmerber, G.; Bowen, M.; Boukari, S.; Beaurepaire, E.; Dreiser, J.; Ruben, M. Engineering On-Surface Spin Crossover: Spin-State Switching in a Self-Assembled Film of Vacuum-Sublimable Functional Molecule. *Adv. Mater.* **2018**, *30* (11), 1705416.

(83) Galadzhun, I.; Kulmaczewski, R.; Cespedes, O.; Yamada, M.; Yoshinari, N.; Konno, T.; Halcrow, M. A. 2,6-Bis(pyrazol-1-Yl)pyridine-4-carboxylate Esters with Alkyl Chain Substituents and Their Iron(II) Complexes. *Inorg. Chem.* **2018**, *57* (21), 13761−13771.

(84) Feltham, H. L. C.; Johnson, C.; Elliott, A. B. S.; Gordon, K. C.; Albrecht, M.; Brooker, S. Tail" Tuning of Iron(II) Spin Crossover Temperature by 100 K. *Inorg. Chem.* **2015**, *54* (6), 2902−2909.

(85) Kitchen, J. A.; White, N. G.; Gandolfi, C.; Albrecht, M.; Jameson, G. N. L.; Tallon, J. L.; Brooker, S. Room-temperature spin crossover and Langmuir−Blodgett film formation of an iron(II) triazole complex featuring a long alkyl chain substituent: the tail that wags the dog. *Chem. Commun.* **2010**, *46* (35), 6464−6466.

(86) Rosario-Amorin, D.; Dechambenoit, P.; Bentaleb, A.; Rouzières, M.; Mathonière, C.; Clérac, R. Multistability at Room

Temperature in a Bent-Shaped Spin-Crossover Complex Decorated with Long Alkyl Chains. *J. Am. Chem. Soc.* **2018**, *140* (1), 98−101.

(87) Seredyuk, M.; Muñoz, M. C.; Castro, M.; Romero-Morcillo, T.; Gaspar, A. B.; Real, J. A. Unprecedented Multi-Stable Spin Crossover Molecular Material with Two Thermal Memory Channels. *Chem. - Eur. J.* **2013**, *19* (21), 6591−6596.
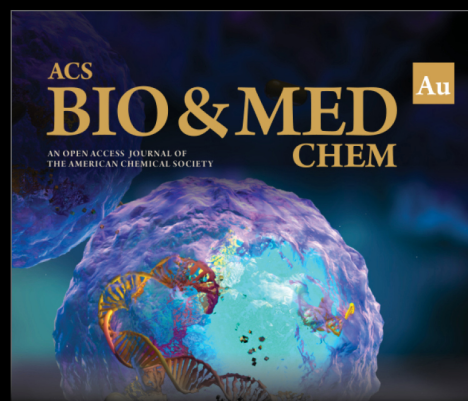
(88) Sheldrick, G. M. *SHELXT* − Integrated space-group and crystal-structure determination. *Acta Crystallogr. Sect. Found. Adv.* **2015**, *71* (1), 3−8.

(89) Sheldrick, G. M. A short sistory of *SHELX. Acta Crystallogr. A* **2008**, *64* (1), 112−122.

(90) Soler, J. M.; Artacho, E.; Gale, J. D.; García, A.; Junquera, J.; Ordejón, P.; Sánchez-Portal, D. The SIESTA method for *ab Initio* order- *N* materials simulation. *J. Phys.: Condens. Matter* **2002**, *14* (11), 2745−2779.

(91) Perdew, J. P.; Burke, K.; Ernzerhof, M. Generalized Gradient Approximation Made Simple. *Phys. Rev. Lett.* **1996**, *77* (18), 3865−3868.

(92) Ferrer, J.; Lambert, C. J.; García-Suárez, V. M.; Manrique, D. Z.; Visontai, D.; Oroszlany, L.; Rodríguez-Ferradás, R.; Grace, I.; Bailey, S. W. D.; Gillemot, K.; Sadeghi, H.; Algharagholy, L. A. GOLLUM: a next-generation simulation tool for electron, thermal and spin transport. *New J. Phys.* **2014**, *16* (9), 093029.